INSTITUT DE FRANCE
Académie des sciences

Comptes Rendus

Chimie

J. Brahmi, S. Nasri, H. Saidi, K. Aouadi, M. R. Sanderson, M. Winter, D. Cruickshank, S. Najmudin and H. Nasri

Optical and photoelectronic properties of a new material: Optoelectronic application

Volume 23, issue 6-7 (2020), p. 403-414

Published online: 10 November 2020

https://doi.org/10.5802/crchim.20

Les Comptes Rendus. Chimie *sont membres du*
Centre Mersenne pour l'édition scientifique ouverte
www.centre-mersenne.org
e-ISSN : 1878-1543

Comptes Rendus
Chimie
2020, 23, nº 6-7, p. 403-414
https://doi.org/10.5802/crchim.20

Preliminary communication / *Communication préliminaire*

Optical and photoelectronic properties of a new material: Optoelectronic application

J. Brahmi[*, a], S. Nasri[*, a, b], H. Saidi[c], K. Aouadi[d, e], M. R. Sanderson[f], M. Winter[g], D. Cruickshank[h], S. Najmudin[f] and H. Nasri[a]

[a] University of Monastir, Laboratoire de Physico-chimie des Matériaux, Faculté des Sciences de Monastir, Avenue de l'environnement, 5019, Monastir, Tunisia

[b] Chemistry Department, College of Science Al-Zulfi, Majmaah University, Saudi Arabia

[c] University of Monastir, Laboratoire de la Matière Condensée et des Nanosciences, Faculté des Sciences Monastir, Avenue de l'Environnement, 5019, Monastir, Tunisia

[d] Faculty of Sciences, University of Monastir, Avenue de l'environnement, 5029 Monastir, Tunisie

[e] Department of Chemistry, College of Science, Qassim University, Buraidah 51452, Saudi Arabia

[f] Randall Centre for Cell and Molecular Biophysics, King's College London, 3rd Floor, New Hunt's House, Guy's Campus, London SE1 1UL, UK

[g] Agilent Technologies, Yarnton, Oxfordshire, UK

[h] Rigaku Europe, Unit 44, Monument Park, Chalgrove, Oxfordshire, OX44 7RW, UK

E-mails: jihedbrahmi85@live.fr (J. Brahmi), nn.soumaya@gmail.com (S. Nasri), hamzasaiidi@yahoo.fr (H. Saidi), kaissaouadi@live.fr (K. Aouadi), mark.sanderson@kcl.ac.uk (M. R. Sanderson), winter.M@live.fr (M. Winter), D.Cruickshank@gmail.com (D. Cruickshank), shabir.najmudin@kcl.ac.uk (S. Najmudin), habibnasri@live.fr (H. Nasri)

Abstract. With the aim of studying the optical, electrochemical, and electronic properties of a new porphyrin-based material, we have synthesized a new porphyrinic complex, namely the (4,4′-bipyridine)(*meso*-tetratrifluoromethylphenylporphyrinato)zinc(II) 4,4′-bipyridine disolvate dihydrate complex with the formula [Zn(TFMPP)(4,4′-bipy)]·2(4,4′-bipy)·2H_2O (**I**). This species is characterized by single-crystal X-ray molecular structure. The optical study is performed by UV–visible absorption and fluorescence spectroscopy. The fluorescence intensity presents an emission in the UV–visible range, indicating that this compound can be used as an optoelectronic material. The optical energy gap is 1.95 eV, and the current–voltage characteristics and impedance spectroscopy measurements have been studied to define the electronic properties of the zinc (II) porphyrin complex. The barrier height ϕ_b is calculated, and the space-charge limited current mechanism is found to control the conductance. The results from the electronic study confirm that our porphyrin derivative can be used for various optoelectronic applications.

* Corresponding authors.

Keywords. UV–visible spectroscopy, X-ray molecular structure, Optical gap, Electronic study, Optoelectronic applications.

Manuscript received and accepted 25th February 2020.

1. Introduction

Porphyrinic complexes have become of paramount importance in recent years. They can be applied in several fields such as photovoltaic materials. The imitation of biological energy transfer systems of chlorophyll type has led to the preparation of numerous porphyrinic compounds with electron donor and electron acceptor characteristics [1–4].

Among metalloporphyrins, iron(II), iron(III), and zinc(II) porphyrin coordination species have been the most studied since the late fifties. Synthetic ferrous and ferric porphyrins have been exceptionally investigated mostly because of their very close resemblance to iron proteins and enzymes such as hemoglobin, cytochromes C, and cytochromes P450 for which they were used as models. On the other hand, zinc(II) metalloporphyrins have also been excessively investigated mainly because these species provide simpler systems (where the metal ion is unambiguously in the +II oxidation state) than those of iron, cobalt, or other d transition metals to evaluate the influence of a wide range of different ligands on the physicochemical properties of porphyrin complexes. Then, over the past decade, zinc porphyrin complexes have been involved in a wide range of cutting-edge areas of research. Those include energy storage or conversion, molecular optoelectronics or the field of sensors [5–8], and chemical and biological sensors [9,10].

Our research group has been involved in a number of works on zinc(II) porphyrin complexes. Indeed, the synthesis and the spectroscopic, electrochemical, and structural characterization of these species, as well as some physical and catalytic applications involving these compounds, have been reported [11–16]. In 2019, we reported the synthesis, the IR, the ^{1}H NMR data, the UV–visible titration, the photoluminescence, and the cyclic voltammetry results of the hexamethylenetetramine zinc(II) complex with the electron-deficient *meso*-tetratrifluoromethylphenylporphyrin (H_2TFMPP) having the formula [Zn(TFMPP)(HMTA)] (HMTA = hexamethylenetetramine) [6]. The electronic properties of the [ITO/Porph-Zn/Al] system have been investigated by current–voltage (I–V) and impedance spectroscopy measurements.

In order to better understand the role of H_2TFMPP electron-deficient porphyrin as well as that of the 4,4-bipyridine axial ligand in the optical and the photoelectronic properties of zinc metalloporphyrins, the (4,4′-bipyridine)[*meso*-tetratrifluoromethylphenylporphyrinato]zinc(II) 4,4′-bipyridine disolvate dihydrate complex, with the formula [Zn(TFMPP)(4,4′-bpy)]·2(4,4-bipy)·2H_2O, (**I**) was synthesized and fully characterized by X-ray molecular structure, UV–visible, fluorescence, IR, and NMR spectroscopy. The electronic properties of this species indicated that the title complex can be used in optoelectronic devices. Results of the comparison of these properties with those of the related [Zn(TFMPP)(HMTA)] coordination compound are also reported.

2. Experimental section

2.1. *Materials and methods*

All reagents employed were commercially available and were used as received without further purification. The *meso*-(tetratrifluoromethylphenylporphyrin) (H_2TFMPP) was synthesized according to the literature [17,18]. The [Zn^{II}(TFMPP)] starting material was prepared according to the standard method from the literature [19]. All reactions and manipulations for the preparation of the Zn(II) porphyrin derivative were carried out under aerobic conditions. The UV–visible spectra and titrations were recorded by a WinASPECT PLUS (validation for SPECORD PLUS version 4.2) scanning spectrophotometer. ^{1}H NMR spectroscopic characterization was performed using a Bruker DPX 400 spectrometer. Chemical shifts were reported in ppm downfield from internal tetramethylsilane (TMS).

2.2. *Synthesis of [Zn(TFMPP)(4,4′-bipy)]·(4,4′-bipy)·2H_2O (**I**)*

To a solution of [Zn(TFMPP)] (100 mg, 0.088 mmol) in dichloromethane (5 mL) was added an excess of 4,4′-bipyridine (250 mg, 1.59 mmol). The reaction

mixture was stirred at room temperature for 8 h and then overlaid with n-hexane. Dark purple crystals, of (**I**) suitable for X-ray diffraction, were obtained within 10 days with a yield of about 86%.

Elemental analysis (%) for $C_{78}H_{52}F_{12}N_{10}O_2Zn$: C 60.42, H 3.38, N 9.03%; found: C 60.98, H 3.21, N 9.14%. ^{1}H NMR (400 MHz, $CDCl_3$): δ (ppm) 7.06 (d, 8H, J 6.8 Hz), 8.00 (d, 8H, J 8 Hz), 8.31 (d, 8H, J 8.2 Hz), 8.82 (s, 8H, β-pyrrole-H). UV/vis (CH_2Cl_2), λ_{max} (nm) ($\varepsilon \times 10^{-3}$ L·mmol^{-1}·cm^{-1}) 430 (958), 561 (65), 602 (41).

The chemical reaction in the preparation of [Zn^{II}(TFMPP)(4,4′-bipy)]·2(4,4′-bipy)·H_2O (**I**) is shown in Scheme 1.

2.3. *X-ray structure determination*

Crystallographic data and selected bond lengths and angles for (**1**) are listed in Table 1 and Supplementary Table 1, respectively. Intensity data were collected at 100 (2) K on an XtaLAB Synergy, Dualflex, HyPix area-detector diffractometer using graphite-monochromated Mo Kα radiation (λ = 0.71073 Å). The reflections were scaled and corrected for absorption effects with SCALE3 ABSPACK in the CrysAlisPRO program [20]. The crystalline structures were solved by direct methods using SIR-2004-1.0 [21] and refined by full-matrix least squares on $|F|^2$ using the SHELXL-97 program [22]. All non-hydrogen atoms were refined anisotropically. The H atoms for (**I**) were included at estimated positions using a riding model except in the case of the free water molecule, where the H atoms were located using the CALC-OH program [23,24].

3. Results and discussion

3.1. *UV–visible absorption*

The absorption spectrum of the synthesized porphyrinic complex (4,4′-bipyridine)(*meso*-tetratrifluoromethylphenylporphyrinato)zinc(II) 4,4-bipyridine disolvate dihydrate with the formula [Zn(TFMPP)(4,4′-bpy)]·2(4,4′-bipy)·2H_2O (**I**) is characteristic of a zinc(II) pentacoordinated *meso*-porphyrin coordination compound with a Soret band (B-band) at 430 nm and a Q-band in the range 560–610 nm (Figure 1) [13].

The difference in energy between the highest occupied molecular orbital (HOMO) and the lowest unoccupied molecular orbital (LUMO), obtained from the UV–visible spectra, defines the optical gap energy (E_g). The E_g value was calculated by the Tauc plot method [25] using the relation

$$(\alpha h\nu)^2 = c(h\nu - E_g),$$

where α is the absorption coefficient of the material, c is a constant, and $h\nu$ is the photonic energy. The calculated E_g value for (**I**) is 1.95 eV, which is normal for a metalloporphyrin species.

3.2. *Fluorescence spectroscopy*

Porphyrins and metalloporphyrins have very interesting photophysical properties thanks to the electronic conjugation of the aromatic ring. Figure 2 illustrates the fluorescence spectra of our synthetic zinc complex recorded in dichloromethane at room temperature. Following laser excitation (λ_{exc} = 500 nm) of a dichloromethane solution of (**I**), an electron of the HOMO is excited to the LUMO, which leaves a hole in the highest orbital (HOMO). This hole can be filled by a fast intramolecular electron transfer. This phenomenon provides a mechanism for non-radiative deactivation of the excited state. These results show that the complex (**I**) can be used for various optoelectronic applications such as a priori Organic Light-Emitting Diode (OLED) and Organic Photovoltaics (OPV) structures.

The fluorescence spectrum of (**I**) presents two emission bands: Q(0,0) and Q(0,1) with λ_{max} values at 599 and 650 nm, respectively.

3.3. *X-ray molecular structure*

The title compound crystallizes in the monoclinic space group with the *C2/c* space group. The asymmetric unit of (**I**) is made up of one half [Zn(TFMPP)(4,4′-bipy)] molecule, one free 4,4′-bipyridine molecule, and one water molecule. Figure 3 is an ORTEP (Oak Ridge Thermal Ellipsoid Plot) diagram of the complex (**I**).

The coordination geometry around the Zn(II) in **(I)** is square-pyramidal, where the four N-donor

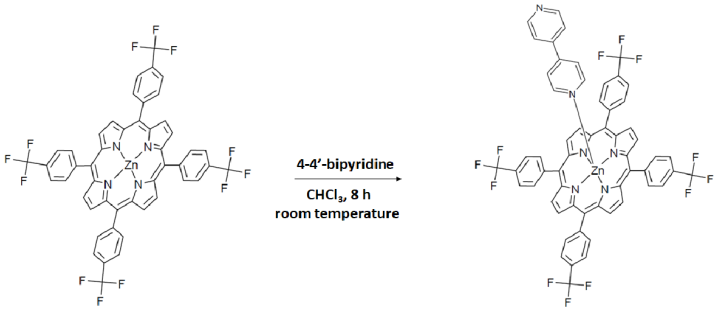

Scheme 1. Synthesis of [Zn(TFMPP)(4,4′-bipy)]·2(4,4′-bipy)·2H_2O (**I**).

Table 1. Crystal and refinement data of [Zn^{II}(TFMPP)(4,4′-bipy)]·2(4,4′-bipy)·2H_2O(**I**)

Compound	**(I)**
Empirical formula	$C_{78}H_{52}F_{12}N_{10}O_2Zn$
Formula weight (g·mol^{-1})	1450.70
Crystal system	Monoclinic
Space group	C2/c
a (Å)	16.0350(5)
b (Å)	18.7235(5)
c (Å)	21.6904(6)
β (°)	101.845(3)
V (Å^3)	6373.5(3)
Z	4
μ (mm^{-1})	0.481
F(000)	2976
Crystal size (mm^3)	0.64 × 0.40 × 0.27
T (K)	100 (2)
Θ range (°)	2.073–26.372
Limiting indices	$-20 \le h \le 20$, $-23 \le k \le 23$, $-27 \le l \le 27$
Reflec. collec./unique/observed	28933/6450/5890
Parameters	469
S (goodness of fit)	1.086
R_1, wR_2 (Fo > 4σ(Fo))	0.0332, 0.0861
R_1, wR_2 (all data)	0.0371, 0.0919
Min./max. res. (eÅ^{-3})	−0.435/0.374
CCDC	1940323

atoms from the pyrrole rings of the TFPP porphyrinato occupy equatorial positions along the porphyrin core while one N-donor atom of the 4,4′-bipyridine species occupies the axial position (Figure 3). A search of the Cambridge Structural Database (CSD, Version 5.40) [26] has shown that the majority of the reported structures of zinc metalloporphyrins with 4,4′-bipyridine are either dimers or polymers and very few are five-coordinated (Table 2).

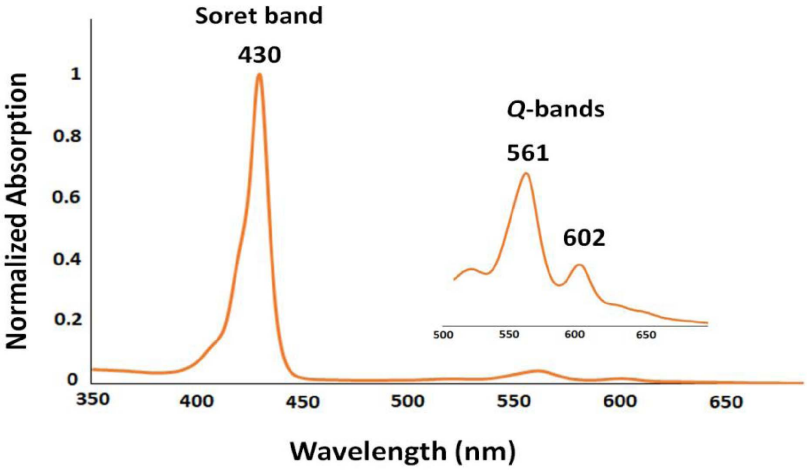

Figure 1. UV–visible absorption spectrum of [Zn(TFMPP)(4,4′-bipy)]·2(4,4′-bipy)·2H_2O (**I**) recorded in dichloromethane at concentrations of approximately 10^{-6} M.

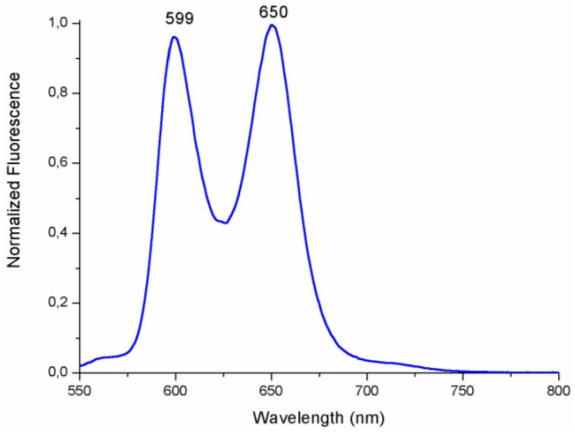

Figure 2. Normalized fluorescence spectra of [Zn(TFMPP)(4,4′-bipy)]·2(4,4′-bipy)·2H_2O (**I**) in dichloromethane (concentration ~10^{-6} M). The excitation wavelength is 500 nm.

The distance between the Zn(II) center metal and the nitrogen atom of the 4,4′-bipyridine axial ligand (Zn–N(4,4′-bipy)) for our complex (**I**) is 2.1295(18) Å, which is slightly shorter than that for the related TEBOP derivative (Zn–N(4,4′-bipy) = 2.152 Å). The Zn–N(4,4′-bipy) values for the reported 4,4′-bipy zinc(II) porphyrins are in the (2.129–2.371) Å range (Table 2).

The dihedral angle (ϕ) between the two pyridyl groups of the 4,4′-bipyridine axial ligand for (**I**) is 42.09°, which is in the (0.0°–47°) range for the reported (4,4′-bipy)-zinc(II) porphyrin complexes. The average equatorial zinc–nitrogen pyrrole distance (Zn–N_p) of (**I**), which is 2.080(2) Å, is in the (2.032–2.081) Å range of the reported [Zn(Porph)(4,4′-bipy] moieties (Table 2).

Figure 4 depicts the formal diagram of the porphyrinato cores of (**I**), showing the displacements of each atom from the mean plane of the 24 atoms of the porphyrin macrocycle ion in units of 0.01 Å. The porphyrin macrocycle of our 4,4′-bipy derivative exhibits major *ruffling*, as indicated by the high values of the displacement of the *meso*-carbon atoms above and below the porphyrin mean plane and a major *saddle* deformation (alternative displacements of pyrrole rings above and below the porphyrin mean plane). Moreover, the displacement of the zinc central metal from the mean plane of the porphyrin core (P_C) is 0.4231(5) Å. This Zn–P_C distance is quite longer than those of the *meso*-arylporphyrin type [Zn(Porph)(4,4′-bipy)] complexes (Porph = *meso*-arylporphyrin) but shorter than that of the [Zn(OEP)(4,4′-bipy)], where OEP is the β-pyrrole substituted octaethylporphyrinato.

The crystal packing of (**I**) is made up of pairs of layers parallel to the *c* axis (Figure 5). Within a pair of layers, the two-dimensional sheets are linked together via weak intermolecular interactions of type C–H···F between the F1 atom of one TFPP porphyrinato and the hydrogen of the carbon C15 of a phenyl ring of a

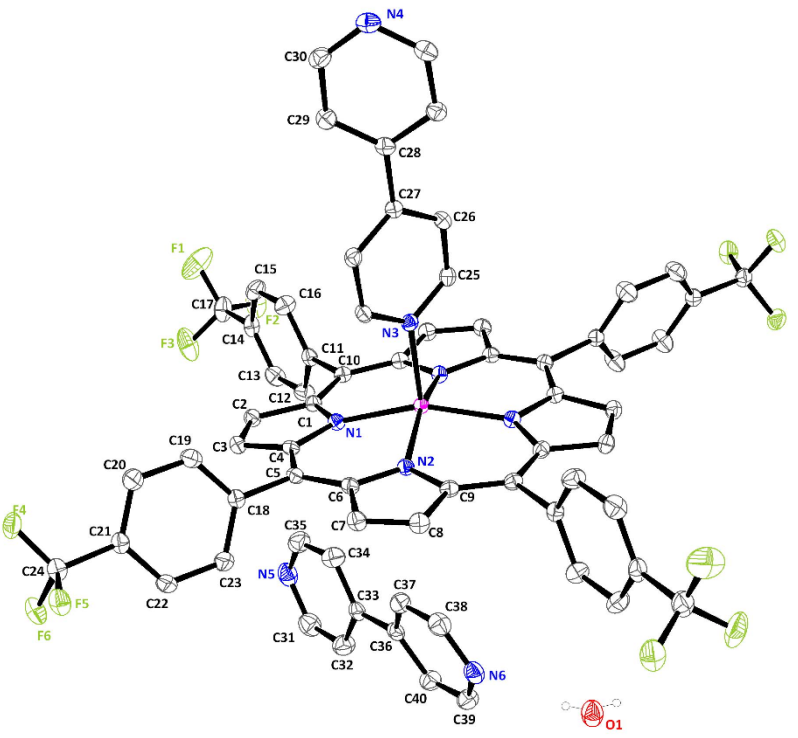

Figure 3. ORTEP diagram of [Zn(TFMPP)(4,4′-bpy)]·(4,4′-bipy)·H_2O with the atom-numbering scheme. Displacement ellipsoids are drawn at the 40% probability level. H atoms have been omitted for clarity.

porphyrin of the second sheet with a C15–H···F1 distance of 3.231(2) Å (Supplementary Table 2).

The two-dimensional layer is stabilized via the following interactions (Figure 6): (i) two free 4,4′-bipyridine molecules are linked together by weak π–π interactions between the centroids of two pyridyl rings at a Cg···Cg distance of 3.6771(11) Å (Supplementary Table 3), (ii) the nitrogens N5 and N6 of two pairs of the two free 4,4′-bipy molecules are H-bonded to a water molecule with the O1–H1O1···N5 and the O1–H2O1···N6 interactions at distances of 2.984(2) and 2.937(2) Å, respectively, (iii) the oxygen atom O6 of the same water molecule is involved in a weak non-conventional H bond with the hydrogen of the carbon C26 of a phenyl porphyrinato ring of a nearby [Zn(TFPP)(4,4′-bipy)] molecule at a C26–H28···O6 distance of 3.163(2) Å, and (iv) the carbon C20 of a phenyl porphyrin and the centroid Cg1 of the pyrrole N1/C1–C4 are involved in a C–H···Cg intermolecular interaction at a C20-H20···Cg1 distance of 3.638(2) Å.

4. Electronic study

In this study, devices consist of an active layer composed of the porphyrin complex (**I**) located between ITO-coated glass and the aluminum contact. In order to ensure good quality of the film surface, an AFM image was recorded, displaying a uniform thin film with a very good layered structure (1.98 nm).

Complexe (**I**) has important electronic properties and an optical gap energy of the order of that of semiconductors. The *I*–*V* measurements were conducted between −1 and 1 V using the Keithley 236 measurement unit and the impedance measurements were performed using an impedance analyzer (Hewlett Packard 4192ALF). The electronic characterization of the diode structure is an important way to provide useful information about transport properties in organic materials.

Figure 7 displays the *I*–*V* curve measured at room temperature for ITO/P**i**/Al (P**i** = [Zn(TFMPP)(4,4′-bipy)]·2(4,4′-bipy)·$2H_2O$, which shows a behavior

Table 2. Selected bond lengths (Å) and angles (°) for several zinc(II) porphyrinic and non-porphyrinic complexes

Complex	Zn–N_p [a]	Zn–N_L [b]	Zn–P_C [c]	ϕ [d]	Ref.
Zinc(II) porphyrin complexes					
$[Zn^{II}(TBPP)(pipz)]$ [e,f]	2.078(7)	2.078(7)	0.4365(4)	-	[27]
[Zn(TPBP)(dabco)] [e,g]	2.078(2)	2.185(2)	0.4324(5)	-	[27]
$[\{Zn(TPBP)\}_2(\mu_2\text{-dabco})]$ [e,g]	2.075(4)	2.182(4)	0.4151(1)	-	[27]
$[Zn(TPBP)(pyz)_2]$ [e,h]	2.027(3)	2.459(5)	0.012(2)	-	[27]
Zinc(II) 4,4′-bipyridine porphyrin complexes					
$[\{Zn(TPP)\}_2(\mu_2\text{-}4,4'\text{-bpy})]$ [i]	2.081(2), 2.065(1)	2.169(6), 2.270(7)	0.327, 0.286	46.86	[28]
$\{[Zn(TPP)]_3(\mu_2\text{-}4,4'\text{-bpy})\}_2$ [i]	2.049(8), 2.058	2.185(8), 2.490	-	21.63 23.61	[28]
$[\{Zn(TOHPP)\}_2(\mu_2\text{-}4,4'\text{-bpy})]$ [k]	2.032, 2.097	2.134, 2.144	0.306, 0.308	3.05	[29]
$[\{Zn(OEP)\}_2(\mu_2\text{-}4,4'\text{-bpy})]$ [l]	2.080(3)	2.173(4)	0.517	0.0	[30]
$[\{Zn(TPBP)\}_2(\mu_2\text{-}4,4'\text{-bpy})]$ [e]	2.063(6)	2.178(6)	0.329(2)	0.0	[13]
[Zn(TFMPP](4,4′-bipy)]	2.080(2)	2.1295(18)	0.4231(5)	42.09	t.w.

[a]: Zn–N_p = average equatorial M–$N_{pyrrole}$ distance,
[b]: Zn–N_L = distance between Zn(II) and the nitrogen atom of the N-donor ligand,
[c]: Zn–P_C = distance between Zn(II) and the 24-atom mean plane,
[d]: ϕ = dihedral angle between the two pyridyl groups of the 4,4′-bipy axial ligand,
[e]: pipz = piperazine ligand,
[f]: TBPP = *meso*-tetrakis-[4-(benzoyloxy)phenyl]porphyrinato,
[g]: dabco = 1,4-diazabicyclo[2.2.2]octane ligand,
[h]: pyz = pyrazine ligand,
[i]: TPP = *meso*-tetraphenylporphyrinato,
[k]: TOHPP = *meso*-tetrakis(4-hydroxyphenyl)porphyrinato,
[l]: OEP = octaethylporphyrinato.

typical of that of the forward and reverse bias diode. The value of the threshold voltage is about 0.53 V.

According to the shape of the *I*–*V* curve, there are two different regimes depending on the voltage. In the first regime, for high voltages, the electronic *I*–*V* curve exhibits an asymmetrical characteristic, which might result from the injection manner of the electrons and holes into the barriers. This is due to the difference between the work functions of the cathode and the anode. In the second regime, for low voltages, the *I*–*V* curve shows a symmetric characteristic, which can be explained by the localized state with defects inducing localized gap states [31].

In order to calculate the barrier height and the saturation current values, the *I*–*V* curve is presented on a semi-logarithmic scale. As shown in Figure 8, the behavior of the current versus the potential is sensitive to the presence of the series resistance R_s related to wires and contact, the shunt resistance R_{sh}, and to the interface states. The effective barrier height Φ_b and the saturation current I_s are calculated using (1) [32]:

$$\Phi_b = \frac{K \cdot T}{q} \ln\left(\frac{S \cdot A^* \cdot T^2}{I_s}\right). \quad (1)$$

Here K is the Boltzmann constant (1.38×10^{-23} J·K^{-1}), A^* is the Richardson effective constant (120 A·cm^{-2}·K^{-2}), T is the room temperature, and q refers to the electronic charge.

From this investigation, we conclude that the system containing the [Zn(TFMPP)(4,4′-bipy)]·2(4,4′-bipy)·2H_2O complex exhibits a barrier height of 1.2533 V and a saturation current (I_s) of 6.027×10^{-9} A (Figure 8 and Table 3).

Based on these results and in comparison with those of the related species complex

Table 3. Electrical parameters of the [TiO/Pi/Al] system

Complex	I_s (A)	ϕ_b (V)
[Zn(TFMPP)(4,4′-bipy)]·2(4,4′-bipy)·2H_2O	6.027×10^{-9}	1.2533

Figure 4. Schematic representation of the porphyrin macrocycle of the [Zn(TFMPP)(4,4′-bipy)] complex showing the displacements of each atom from the 24-atom mean plane in units of 0.01 Å.

[Zn^{II}(TFMPP)(HMTA)], we note that our complex (**I**) has a high barrier height ϕ_b compared to the related zinc-HMTA derivative. This is most probably due to the aromatic ligand 4,4′-bpy for (**I**), which can prevent the distribution of the charge contrary to the case of the related species containing the non-aromatic ligand HMTA.

It is the same for the saturation current 6.027×10^{-9} for our zinc(II)-4,4′-bipy derivative, which is very low compared to that of the related [Zn^{II}(TFMPP)(HMTA)] complex whose value is equal to 6.57×10^{-6}. These results show that the nature of the axial ligand plays a very important role in the optoelectronic properties for this type of porphyrin compound.

The variation of I as a function of V has been represented in a log–log plot to better study the mechanism of electrical conductance across the junction (Figure 9).

For complex (**I**), as shown by this figure, there are different regions where the current varies as a function of the potential according to the relation $I \approx V^m$, where m represents the slope for each region and provides information about the type of conduction mechanism.

The slope value is close to unity at low voltage defining the ohmic region. In this region, the presence of a small amount of interface barrier hinders charge injection. In this case, the density of thermally excited load carriers is insufficient and trap levels are empty [32]. The current density is given by (2):

$$J_\Omega = q \cdot p_o \cdot \mu \cdot \frac{V}{d}. \tag{2}$$

Here q is the electronic charge, μ is the charge mobility, p_o is the free carrier density, d is the film thickness and V is the applied voltage.

The slope value is approximately 1.6 at medium voltage in the case of our zinc porphyrin complex, where the voltage follows the power law dependence (I–V), which is related to the space-charge limited current mechanism (SCLC). Moreover, the density of the injected charges from electrodes increases. Since the applied voltage passes through the transition voltage V = 0.53 V, the density of the injected charges will dominate the transport capacity of the [Zn(TFMPP)(4,4′-bipy)]·(4,4′-bipy)·2H_2O layer. In this regime, the current density varies following equation (3):

$$J_{SCLC} = \frac{9}{8}\varepsilon \cdot \mu_{eff} \cdot \frac{V^2}{d^3}. \tag{3}$$

Here ε is the material permittivity (assumed to be $4\varepsilon_o$, where ε_o is the vacuum permittivity) and μ_{eff} is the effective carrier mobility equal to $\theta\mu \cdot \theta$, which is the free charge fraction with $\theta = p/(p + p_t)$. Parameters p and p_t represent the free and trapped charge-carrier densities, respectively; d is the film thickness and V is the applied voltage.

According to the SCLC model (3), μ_{eff} for the film containing complex (**I**) was calculated with a value of 0.45 (10^{-5} cm^2/Vs). This result is comparable to the literature value of about 10^{-5} cm^2/Vs for the 2,7-distyrylcarbazole p-type species [33–35].

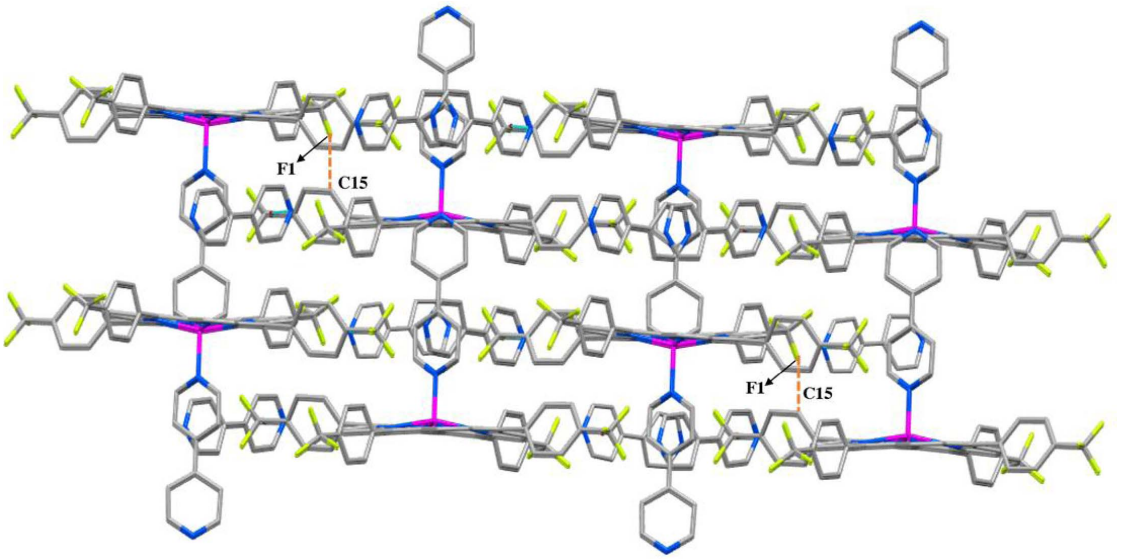

Figure 5. Projection of the crystal lattice of (**I**) down the *c* axis.

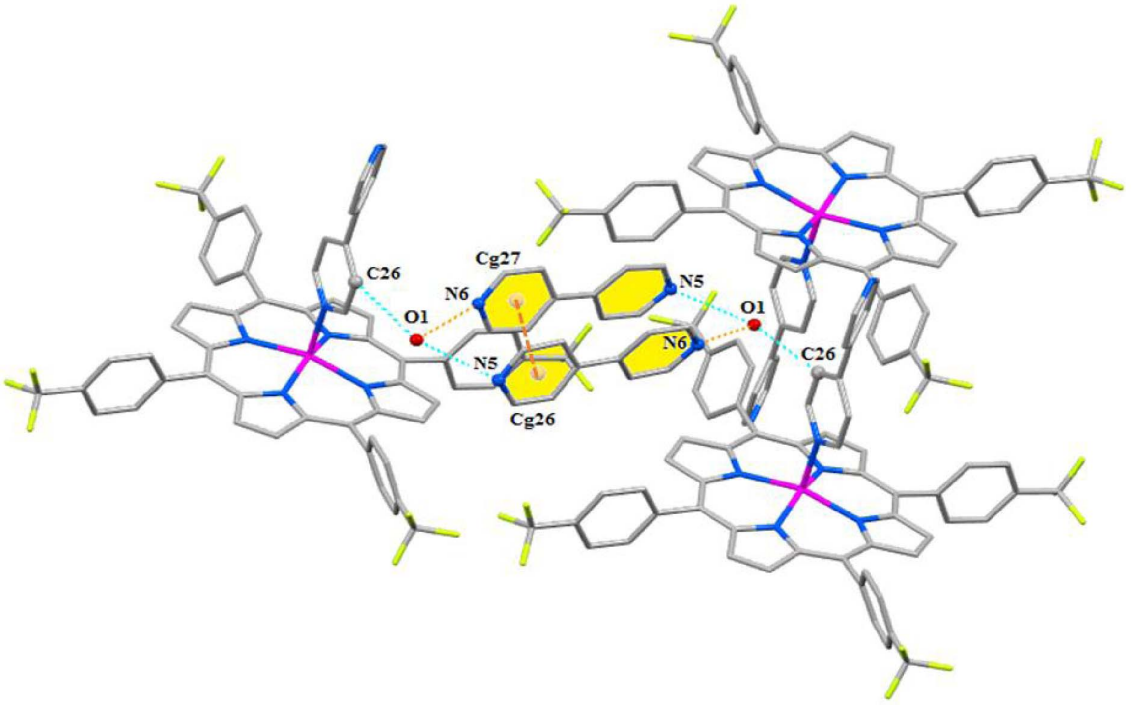

Figure 6. Packing showing the intermolecular interactions within one layer of (**I**).

For high voltages, we observed the third linear region, where the slope value of m is 2.7, which represents the trapped charge limiting current (TCLC) region, where the trap distributions vary exponentially. In this case, trapping levels will affect the transition from the SCLC mechanism to the TCLC mechanism.

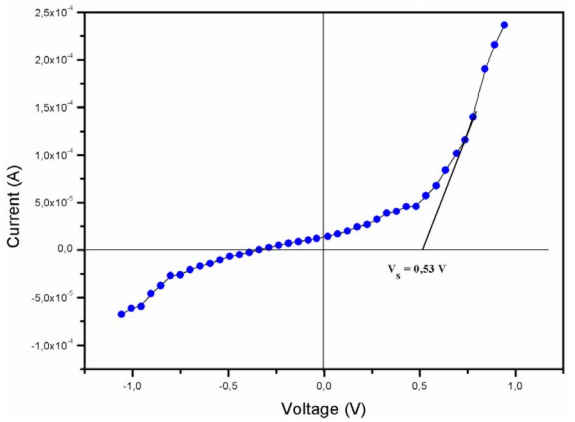

Figure 7. (I–V) characteristics of ITO/[Zn(TFMPP)(4,4′-bipy)]·2(4,4′-bipy)·2H_2O/Al system.

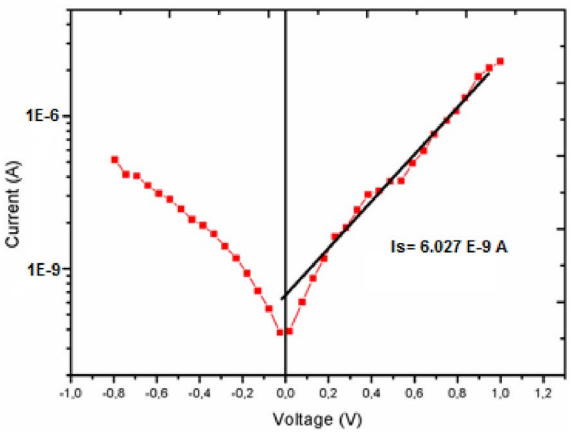

Figure 8. Current–voltage curves of [ITO/ZnPi/Al] (P**i** = (**I**)) in semi-logarithmic representation.

This transition occurs when the injected carrier density exceeds the free carrier density.

As shown by Figure 9, we noticed that both the shape of the curve and the current I values as functions of the voltage V values are very different from those of the related Zn(II)-HMTA species [6]. Moreover, the latter species exhibits better optoelectronic properties that those of our Zn(II)-4,4′-bpy derivative.

4.1. *Impedance spectroscopy*

Complex impedance spectroscopy is a powerful tool to study the dielectric properties of materials [36–38].

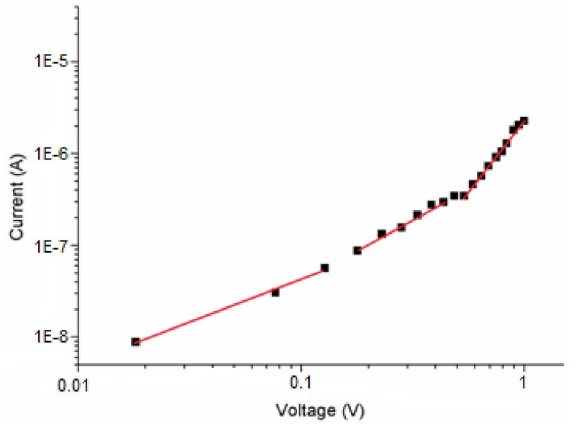

Figure 9. Log–log I–V curve for the [TiO/P**i**/Al] (Pi = (I)) device.

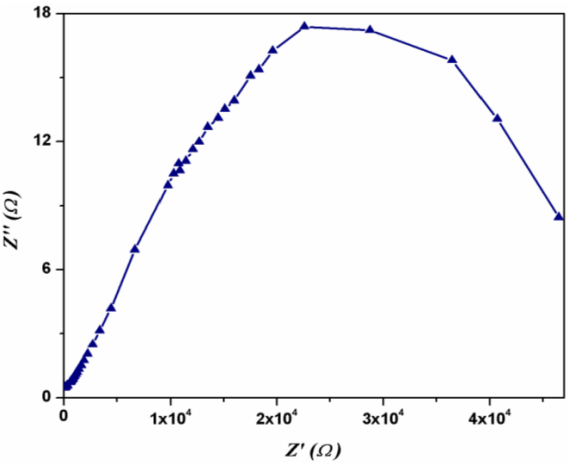

Figure 10. Nyquist plot of the [TiO/Pi/Al] device.

The complex impedance $Z(\omega)$ is divided into two parts: the real part ($\mathrm{Re}(Z) = Z'$) and its imaginary part ($\mathrm{Im}(Z) = Z''$). The $Z(\omega)$ impedance of the [TiO/Pi/Al] system (Pi = complex (**I**)) can be defined as a function of frequency according to (4):

$$Z(\omega) = \mathrm{Re}(Z) + j\mathrm{Im}(Z) = Z'(\omega) + jZ''(\omega). \quad (4)$$

The Nyquist plot of the [TiO/Pi/Al] containing the [Zn(TFMPP)(4,4′-bipy)]·2(4,4′-bipy)·2H_2O film appears as a semicircle. This response indicates the homogeneous nature of the electrode–organic interface. The high-frequency response may contain clues to transport and series resistance elements as well as dielectric contributions (Figure 10).

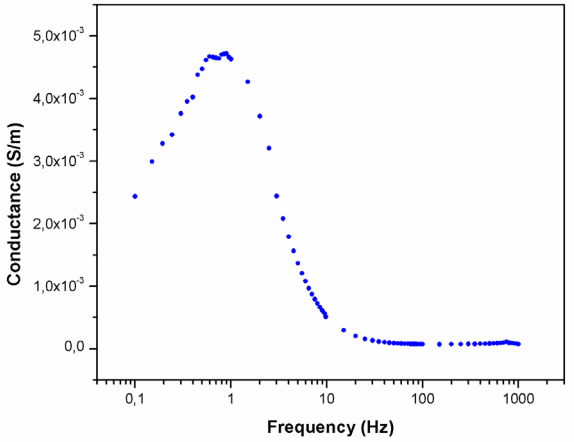

Figure 11. Conductance curve of the [TiO/Pi/Al] device.

4.2. *Conductance*

The conductance curve shows two peaks at low and high frequencies (Figure 11). The conductance of complex (**I**) at low frequency is 4.7×10^{-3} S/m. At low frequency, the conductance depends strongly on the frequency, which is characteristic of a disordered system. However, at high frequency, the conductance tends to zero, where the dipoles ignore the frequency. The switch from the frequency-dependent to the frequency-independent regions is related to the hopping transport mechanism because dipoles will be oriented with the applied field, leading to an increase in charge hopping.

5. Conclusion

In conclusion, we report the synthesis of a new material based on the porphyrin species, which is characterized by UV–visible, fluorescence spectroscopy, and X-ray molecular structure. From the optical gap energy value calculated, it is clear that this material can be used in organic light-emitting diode structures. To investigate the transport characteristics of the [ITO/P**i**/Al] (P**i** = complex (**I**)) diode structure, current–voltage and electrical impedance measurements were carried out. The comparison of the electronic parameter values obtained in the case of our Zn-4,4′-bpy derivative with those of the already known derivative Zn-HMTA (hexamethylenetetramine) with the same *meso*-tetratrifluoromethylphenylporphyrin shows a clear difference between these values, which clearly indicated that the optoelectronic properties of the zinc(II) porphyrin complexes do not depend on the nature of the *meso*-arylporphyrin but rather on the nature of the axial ligand coordinated to the zinc(II).

Acknowledgments

The authors acknowledge Rigaku/Oxford Diffraction for X-ray crystallographic data collection on their Synergy system. They thank Diamond Light Source for access to beamlines I03, I02, I04, I04-1, and I24 (MX1220, MX7656, and MX9495) and the beamline staff for their help, which contributed to the results presented here. This research was supported by PTC Therapeutics Inc. and in part by funding from a Welcome Trust Seeding Drug Discovery award (097753) to PTC Therapeutics. The research was also funded by Biotechnology and Biological Research Council project grants BB/H00405X/1 and BB/K10069/1. X-SP and IL were funded by the BBSRC.

The authors extend their appreciation to the deanship of Scientific Research at Al-Majmaah University and the Ministry of Higher Education and Scientific Research of Tunisia.

Supplementary data

Supporting information for this article is available on the journal's website under https://doi.org/10.5802/crchim.20 or from the author.

References

[1] H. Imahori, S. Hayashi, H. Hayashi, A. Oguro, S. Eu, T. Umeyama, Y. Matano, *J. Phys. Chem. C*, 2009, **113**, 18406-18411.
[2] M. Speck, H. Kurreck, M.-O. Senge, *Eur. J. Org. Chem.*, 2000, 2303-2314.
[3] C.-L. Mai, W.-K. Huang, H.-P. Lu, C.-W. Lee, C.-L. Chiu, Y.-R. Liang, W.-G. Eric Diau, C.-Y. Yeh, *Chem. Comm.*, 2010, **46**, 809-811.
[4] V. Srinivasan, N. Pavithra, S. Anandan, M. Jaccob, A. Kathiravan, *J. M. Struct.*, 2017, **1134**, 112-120.
[5] A.-W. Nevin, G. A. Chamberlain, *J. Appl. Phys.*, 1991, **69**, 4324-4332.
[6] J. Brahmi, S. Nasri, H. Saidi, H. Nasri, K. Aouadi, *Chem. Select.*, 2019, **4**, 1350-1359.
[7] Y. Ding, W. H. Zhu, Y. Xie, *Chem. Rev.*, 2017, **117**, 2203-2256.
[8] D. Khusnutdinova, A. M. Beiler, B. L. Wadsworth, S. I. Jacob, G. F. Moore, *Chem. Sci.*, 2017, **8**, 253-258.

[9] F. C. Gong, D. X. Wu, Z. Cao, X. C. He, *Biosens. Bioelectron.*, 2006, **22**, 423-428.
[10] R. Paolesse, S. Nardis, D. Monti, M. Stefanelli, C. D. Natale, *Chem. Rev.*, 2017, **117**, 2517-2583.
[11] Z. Denden, K. Ezzayani, E. Saint-Aman, F. Loiseau, S. Najmudin, C. Bonifácio, J.-C. Daran, H. Nasri, *Eur. J. Inorg. Chem.*, 2015, 2596-2610.
[12] Z. Denden, W. Harhouri, L. Ben Haj Hassen, Y. Rousselin, E. Saint-Aman, H. Nasri, *J. Mol. Struct.*, 2017, **1133**, 472-478.
[13] S. Nasri, I. Zahou, I. Turowska-Tyrk, T. Roisnel, F. Loiseau, E. Saint-Amant, H. Nasri, *Eur. J. Inorg. Chem.*, 2016, 5004-5019.
[14] R. Soury, M. Jabli, T. A. Saleh, W. S. Abdul-Hassand, E. Saint-Amand, F. Loiseaud, C. Philouze, A. Bujacz, H. Nasri, *J. Mol. Liq.*, 2018, **264**, 134-142.
[15] R. Soury, M. Jabli, T. A. Saleh, W. S. Abdul-Hassan, E. Saint-Aman, F. Loiseau, C. Philouze, H. Nasri, *RSC Adv.*, 2018, **8**, 20143-20156.
[16] J. Brahmi, S. Nasri, H. Saidi, H. Nasri, K. Aouadi, *Chem. Select*, 2019, **4**, 1350-1359.
[17] A. D. Adler, F. R. Longo, J. D. Finarelli, J. Goldmacher, J. Assour, L. J. Korsakoff, *Org. Chem.*, 1967, **32**, 476-476.
[18] S. G. DiMagno, R. A. Williams, M. J. Therien, *J. Org. Chem.*, 1994, **59**, 6943-6948.
[19] J. L. Hoard, K. M. Smith, *Porphyrins and Metalloporphyrins*, Elsevier, Amsterdam, 1975.
[20] Agilent, *CRYSALIS PRO, version 1.171.37.33c*, Agilent Technologies, Wroclaw, Poland, 2014.
[21] A. Altomare, G. Casacarano, C. Giacovazzo, A. Guagliardi, M. C. Burla, G. Polidori, M. Camalli, *J. Appl. Crystallogr.*, 1994, **27**, 435-441.
[22] G. M. Sheldrick, *Acta Crystallogr. C*, 2015, **71**, 3-8.
[23] M. Nardelli, *J. Appl. Crystallogr.*, 1999, **32**, 563-571.
[24] C. C. Ong, V. McKee, G. A. Rodley, *Inorg. Chim. Acta*, 1986, **123**, L11-L14.
[25] J. Tauc, *Mater. Res. Bull.*, 1968, **3**, 37-46.
[26] C. R. Groom, I. J. Bruno, M. P. Lightfood, S. C. Ward, *Acta Crystallogr. B*, 2016, **72**, 171-179.
[27] S. Nasri, K. Ezzayani, I. Turowska-Tyrk, T. Roisnel, H. Nasri, *Acta Crystallogr.*, 2016, **E72**, 937-942.
[28] A. D. Shukla, P. C. Dave, E. Suresh, A. Das, P. Dastidar, *J. Chem. Soc. Dalton Trans.*, 2000, 4459-4463.
[29] Y. Diskin-Posner, G. K. Patra, I. Goldberg, *Chem. Commun.*, 2002, 1420-1421.
[30] D. V. Konarev, S. S. Khasanov, Y. L. Slovokhotov, G. Saito, R. N. Lyubovskaya, *Cryst. Eng. Comm.*, 2008, **10**, 48-53.
[31] S. Hamza, A. Walid, A. Bouazizi, B. R. Herrero, S. Faouzi, *Mater. Res. Express*, 2017, **4**, 18051-18058.
[32] Z. Çaldıran, A. R. Deniz, Ş. Aydoğan, A. Yesildag, D. Ekinci, *Superlattices Microstruct.*, 2013, **56**, 45-54.
[33] A. Jebnouni, M. Chemli, P. Lévêque, S. Fall, M. Majdoub, N. Leclerc, *Org. Electron.*, 2018, **56**, 96-110.
[34] C. A. Amorim, M. R. Cavallari, G. Santos, F. J. Fonseca, A. M. Andrade, S. Mergulhão, *J. Non-Cryst. Solids*, 2012, **358**, 484-491.
[35] S. Hamza, D. Nejeh, A. Walid, B. Abdelaziz, B. Taoufik, G. Regis, *Superlattices Microstruct.*, 2018, **120**, 193-198.
[36] S. Hajra, M. Sahu, V. Purohit, R. N. P. Choudhary, *Helyon.*, 2019, **5**, 1-7.
[37] C. Y. Hao, Z. F. Gu, G. Cheng, L. Li, J. W. Zhang, J. G. Song, Y. F. Yan, M. H. Jiang, *Mater. Elect.*, 2017, **28**, 18357-18365.
[38] C. H. Sameera Devi, M. B. Suresh, G. S. Kumar, G. Prasad, *J. Adv. Dielectr.*, 2012, 1-12.